# Thermal expansion and enthalpies of phase transformation and fusion of $Er_2O_3$ and $Tm_2O_3$ from experiment and computation

*Sergey V. Ushakov*[1], *Qi-Jun Hong*[2*], *Alfred Pavlik III*[1], *Axel van de Walle*[3], *Alexandra Navrotsky*[1*]

[1] Center for Materials of the Universe, School of Molecular Sciences, Arizona State University, Tempe, AZ 85287, USA; anavrots@asu.edu

[2] School for Engineering of Transport, Energy and Matter, Arizona State University, Tempe, AZ; 85287, USA; qhong7@asu.edu

[3] School of Engineering, Brown University, Providence, RI 02912, USA; avdw@brown.edu

**Abstract:**

Erbium and thulium sesquioxides are the only lanthanide oxides which exhibit pre-melting cubic-hexagonal (C-H) phase transformation. The enthalpies of phase transitions and fusion were measured for the first time using a differential thermal analyzer calibrated by melting $Y_2O_3$. C-H transition enthalpies of $Er_2O_3$ and $Tm_2O_3$ are 48 ± 7 and 69 ± 7 kJ/mol at 2301 ± 10 and 2384 ± 14 °C, with enthalpies of fusion 59 ± 9 and 69 ± 8 kJ/mol at 2419 ± 12 and 2416 ± 20 °C, respectively. The mean linear thermal expansion of cubic phases up to transformation temperature was determined from synchrotron diffraction on laser heated aerodynamically levitated $Er_2O_3$ and $Tm_2O_3$ as (8.80 ± 0.02) and (8.74 ± 0.01) $10^{-6}$/K, respectively. The experimental results were used to benchmark ab initio molecular dynamic computations which provided an isobaric heat capacity of 178 ± 5 J/mol/K for both liquid oxides at 2427-3027 °C. The comparable enthalpy values for pre-melting C-H transformation and fusion corroborate a high degree of dynamic disorder in the H phase suggesting superplasticity and ionic conductivity. The melting temperature for cubic $Er_2O_3$ and $Tm_2O_3$ obtained from ab initio molecular dynamic computations aligns with experimentally measured temperature for C-H transition.

## 1. INTRODUCTION

Rare-earth (RE) elements commonly refer to lanthanides, yttrium and scandium. RE oxides are constituents in ceramics for applications ranging from magnetic materials,[1] to thermal barrier coatings,[2] catalysts,[3, 4] and luminescent materials.[5] Thermodynamic description of unary and binary systems is the foundation of calculation of phase diagram (CalPhaD) modeling, which is instrumental for accelerated developments of the new metallic alloys, but still in the database developments stage for ceramics.

Cubic bixbyite-type (*Ia*-3) structure (or C-type after Goldschmidt's classification[6]) is the most stable polymorph for all rare earth sesquioxides at room temperature.[7] With the exceptions of Lu, Yb and Sc oxides, all $RE_2O_3$ undergo several solid-state phase transitions before melting (Fig. 1). Sesquioxides of lanthanides larger than Dy retain their high temperature monoclinic or trigonal structures at room temperature. They were denoted by Goldschmidt as B-type ($C2/m$) and A-type ($P\bar{3}m1$), respectively. The high temperature hexagonal (H, $P6_3/mmc$) and cubic (X, $Im\bar{3}m$) phases cannot be quenched in binary or multicomponent[8, 9] $RE_2O_3$ (however, the reflections assigned to X-phase were identified in $Tm_2O_3$ and $Lu_2O_3$ after irradiation with swift heavy ions (185 MeV Xe)).[10] Thermodynamics of phase transitions involving these phases can only be studied experimentally in situ, which is challenging since they occur above 2000 °C. The H and X notation has been assigned to these phases by Foex and Traverse[11] who discovered them from thermal arrests on $RE_2O_3$ melts solidification and from high temperature X-ray diffraction.

In the thermodynamic assessment performed by Zinkevich[12] enthalpies of fusion and high temperature phase transitions for all $RE_2O_3$ were extrapolated from the measurements performed on $Y_2O_3$ and $Sc_2O_3$ in the 1970s using a custom high temperature drop calorimeter.[13, 14] Several new experimental measurements and computations were performed since the publication of Zinkevich assessment.[12] $La_2O_3$ has the lowest melting temperature in the family (2300 °C). The enthalpies of A-H and H-X phase transitions and fusion of $La_2O_3$ have been measured[15] in a differential thermal analyzer (DTA) calibrated by melting $Al_2O_3$ (Tm 2054 °C)[16] – the only fusion enthalpy standard available for DTA measurements in 2000-2400 °C range. Oxides of Y, Sc, Lu, Yb, Er and Tm have the highest melting temperatures in the family (above 2400 °C).[17] The fusion enthalpies of $Lu_2O_3$ and $Yb_2O_3$ (which do not exhibit pre-melting phase transformations)[18] were measured using drop calorimetry on laser heated samples and computed by DFT and molecular dynamics (MD) methods.[19] New measurements and computations were also performed on $Y_2O_3$.[20]

In this work we report the first measurements of enthalpies of pre-melting phase transformation and fusion of $Er_2O_3$ and $Tm_2O_3$. These are the only binary lanthanide oxides exhibiting high temperature cubic-hexagonal (C-H) transformation. Thermal expansion of C-type $Er_2O_3$ and $Tm_2O_3$ up to the C-H transition temperature have been derived from synchrotron diffraction experiments on laser heated aerodynamically levitated samples. The results are used to benchmark performed ab initio MD computations which have the potential to provide missing thermodynamic data at a faster pace than experiments but still require careful choice of approximations especially for the lanthanides at high temperature.

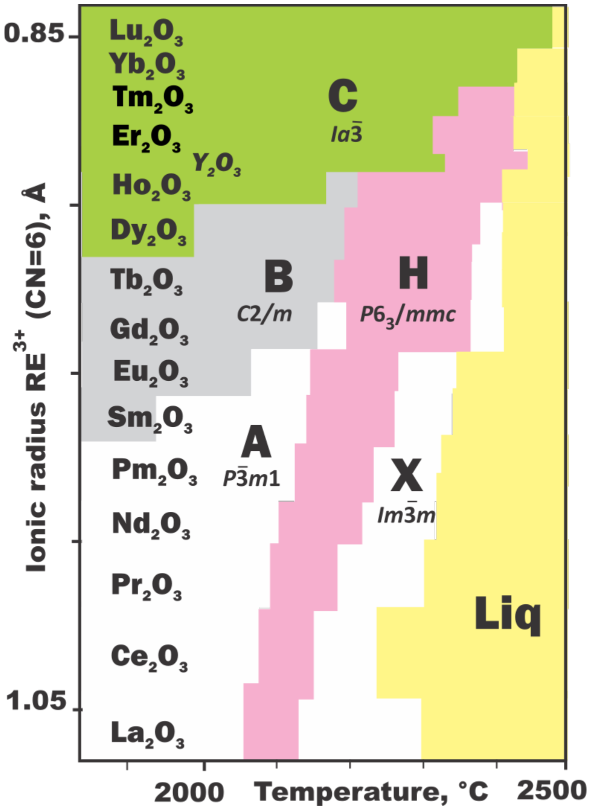

**Figure 1**. High temperature $RE_2O_3$ phases.

## 2. EXPERIMENTAL PROCEDURES

$Er_2O_3$ and $Tm_2O_3$ powders were obtained from Alfa Aesar with metals purity 99.99 %. For high temperature diffraction and thermal analysis measurements samples were laser melted in a copper hearth into spheroids 2-3 mm in diameter. The laser melting setup employs a 400 W $CO_2$ laser and is described in detail elsewhere.[21]

### 2.1 Thermal analysis and electron microscopy

Differential thermal analysis (DTA) experiments were performed using Setaram Setsys 2400 analyzer. The sensor employs W5Re-W26Re (C-type) thermocouples for the sample and furnace temperature and not standard W-W26Re heat flow thermocouples formed by suspension of W holder for sample and reference crucibles on W26Re wires. The instrument was modified by the manufacturer to reach up to 2500 °C; however, the lifetime of the sensors above 2000 °C is limited.

Measurements were performed using a sample thermocouple for temperature control since it shows slower temperature drift. Samples and standards were laser melted into spheroids and sealed in W crucibles under Ar atmosphere to prevent carbon contamination from the furnace protection tube. The details on the instrument and measurement procedures are described elsewhere.[15] After evacuation of the DTA chamber and Ar flow of 40 ml/min had been established, samples were heated at 50 °C/min to 1500 °C, then to the melting temperature at 10 or 20 °C/min heating rate. Temperature and sensitivity calibrations were accomplished by $Y_2O_3$ melting in the same configuration before and after each sample run and described in details in the results section. The baseline runs with empty crucibles were not attempted due to poor baseline reproducibility above 1500 °C. The manual baseline fitting and subtraction has been performed with AKTS Calisto software. The cooling traces on laser melted aerodynamically levitated samples were recorded with FMP2/2X spectropyrometer[22] (FAR Associates).

A Cameca SX-100 electron microprobe was used for samples analysis by energy dispersive spectroscopy and for backscattering electron (BSE) imaging. The analysis was performed on cross-sections of TIG-welded tungsten crucibles recovered after DTA experiments.

## 2.2 X-Ray Diffraction (XRD)

The room temperature unit cell parameters were determined on laser melted samples, powdered and mixed with NIST Si SRM 640c line position standard for powder diffraction. The measurements were performed with a Bruker D2 Phaser diffractometer with Cu $K\alpha1/K\alpha2$ radiation (1.5405/1.5443 Å). High-temperature X-ray diffraction experiments were conducted in transmission geometry at the Advanced Photon Source (APS), Argonne National Laboratory, using an aerodynamic levitator with laser heating system from Materials Developments, Inc., which is available at the beamline 6-ID-D in the user program.[23] Laser-melted spheroids ~2.5 mm in diameter were levitated in argon and oxygen and heated from the top with a 400 W $CO_2$ laser beam. The X-ray beam was shaped to a 500 µm by 200 µm "letterbox" and aimed at the top part of the levitated bead not obstructed by the nozzle. Diffraction images were captured using a Perkin-Elmer XRD 1621 area detector, positioned ~1 m from the sample with a 0.1 s exposure time to prevent saturation. 120 exposures were combined into a single image for further analysis. Levitator software allowed control over gas flow and laser power, with surface temperature monitored by a single band pyrometer (0.9 µm, IR-CAS3CS, Chino Co., Tokyo, Japan) with an emissivity set to 0.92. The gas flow was adjusted to provide constant rotation of the sample. Calibrations of sample to detector distance, beam center, and tilt angle and rotation were performed using a NIST $CeO_2$ powder standard on the surface of a polystyrene bead. The images were integrated from 1 to 10° $2\Theta$ into 1600-point patterns over a 40–160° azimuth not attenuated by the nozzle. Room temperature images were taken before and after heating, with sample displacement refined at room temperature and kept constant for high-temperature refinements using the Pawley[24] method as implemented in GSAS-II package.[25] High temperature data for $Er_2O_3$ and $Tm_2O_3$ were collected during different sessions at APS with X-ray wavelengths of 0.1394(1) and 0.1236(1) Å.

## 3. Computational methods

Density functional theory[26] (DFT) was employed to model $Er_2O_3$ and $Tm_2O_3$. All electronic structures were calculated by the Vienna Ab-initio Simulation Package (VASP)[27], with the projector-augmented-wave (PAW)[28] implementation and the generalized gradient approximation (GGA) for exchange-correlation energy, in the form known as Perdew-Burke-Ernzerhof (PBE).[29] The pseudopotential electronic configuration (with parentheses denoting core states) was

([Kr]$4d^{10}4f^{11}5s^2$)$5p^6 4f^1 6s^2$ with core radius of 1.619 Å for Er, ([Kr]$4d^{10}4f^{12}5s^2$)$5p^6 4f^1 6s^2$ with core radius of 1.650 Å for Tm; for oxygen, the $2s$ and $2p$ electrons were treated as valence with core radius of 0.822 Å. A plane-wave basis set with a 400 eV kinetic energy cutoff was used. First-principles molecular dynamics (MD) techniques were utilized to simulate atomic movements and trajectories in conjunction with the SLUSCHI (Solid and Liquid in Ultra Small Coexistence with Hovering Interfaces) package[30] which automates the process of scripting the calculations with VASP. The electronic temperature was set consistently with the ionic temperature and accounted for by imposing a Fermi distribution upon the electronic density of states. We used automated $k$-meshes generation with a $k$-point density of $15^3$/Å $^{-3}$ in the Brillouin zone. The MD simulations yielding volume and energy per atom as a function of temperature were carried out with 240 atoms under a constant pressure and temperature condition (*NPT*, isothermal-isobaric ensemble) with a time step, typically between 1 and 3 fs. The thermostat was imposed under the Nosé-Hoover chain formalism.[31, 32] The barostat was realized by adjusting the volume every 80 time steps according to average pressure to avoid unphysically large oscillation.[33] The liquid state was achieved by MD simulation of the C-phase at 5727 °C for 0.5 picoseconds, then cooled to the modeling temperature. The length of MD trajectory varied from 8 to 96 picoseconds, depending on convergence rate. On average, computations took about 25,000 CPU hours for volume and enthalpy for each temperature, which required around two weeks on 64 cores of a computer cluster. The metastable melting temperature for C-type $Er_2O_3$ and $Tm_2O_3$ were computed from DFT MD solid–liquid coexistence simulations[34] performed with SLUSCHI code[30] on a cell size of 160 atoms. The method was previously validated in applications to metal alloys,[35] oxides[36] and carbonitride[37] compounds. The computations took approximately 200,000 CPU hours (~20 MD simulations for solid liquid coexistence).

$Er_2O_3$ and $Tm_2O_3$ melting temperatures were also estimated using publicly available[38] graph neural network (GNN) model trained on the database of ~10,000 compounds.[39, 40] The only input required for the model is chemical composition. For the compositions used as part of the training set the model outputs the values in the database along with predicted values with uncertainty. The accuracy of melting temperatures estimated by the GNN model are limited by the accuracy of the training dataset. Hence, the relatively large experimental uncertainties of measured melting temperatures above 2000 °C places limits on the GNN's predictive accuracy at high temperature. The computations with GNN model via web interface[38] took less than a second per composition.

## 4. RESULTS

### 4.1 Differential thermal analysis

Due to frequent DTA sensor failure above 2400 °C, the experiments were performed with two different DTA sensors. Temperature calibration was accomplished from the onsets of endothermic peaks on heating of $Y_2O_3$ corresponding to the C-H transition and melting. The melting temperature of $Y_2O_3$ reported by Foex[41] as 2439 ± 12 °C is an average of the measurements performed in 10 laboratories. The temperature of the C-H transition has been taken as 2347 ± 10 °C based on our prior measurements in a DTA with spectropyrometer.[42] Only data on heating were used for temperature calibration due to undercooling on crystallization and H-C transition in $Y_2O_3$.

Sensitivity calibration was obtained from the integral areas of the heat flow peaks corresponding to C-H transition and melting of $Y_2O_3$. The sum of the enthalpies of C-H transition and melting was taken as 119 ± 10 kJ/mol based on drop-n-catch calorimetry measurements reported earlier.[20] Sensitivity calibration was performed on heating and on cooling. The first experiments were run at a heating rate 20 °C/min to increase signal-to-noise ratio in heat flow trace and to reduce residence time at high temperature and thermocouple aging. However, the C-H transition in $Tm_2O_3$ was not resolved in these conditions. Two melting experiments on $Tm_2O_3$ were accomplished with heating rate 10 °C/min with $Y_2O_3$ calibration before and after experiments. $Er_2O_3$ and $Tm_2O_3$ were observed to remain translucent after DTA experiments, indicating no significant reduction or defect formation after melting in tungsten crucibles. No reaction with W was detected using microprobe analysis and back scattered electron imaging (Fig. 2).

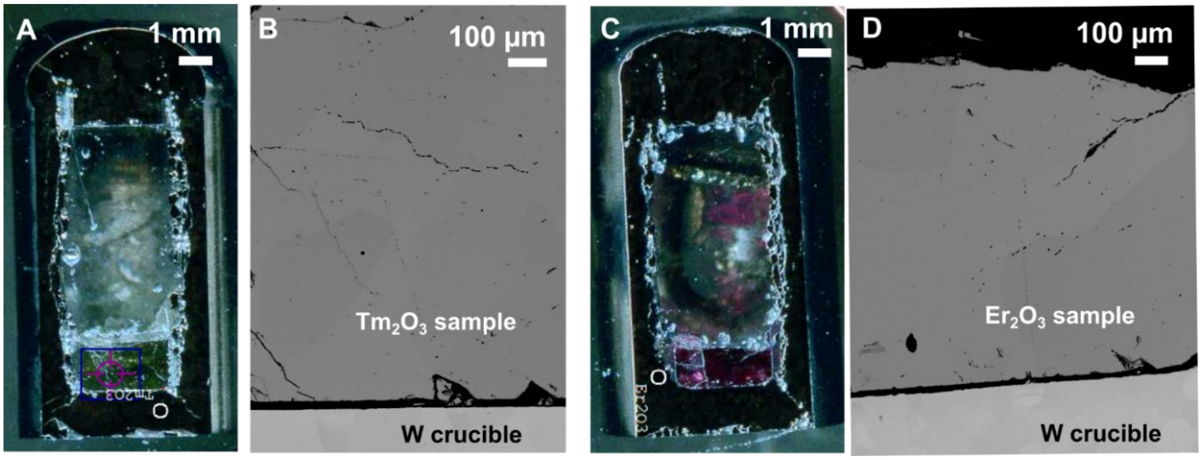

**Figure 2.** (A) and (C): optical photographs of cross section of sealed W crucibles with $Tm_2O_3$ and $Er_2O_3$ samples after differential thermal analysis and embedding in epoxy for microprobe analysis. (B) and (D): back scattered electron (BSE) micrographs of the samples.

The tabulated data for all experiments and calibrations is provided in the supporting information section of this article. The phase transition and melting temperatures for $Er_2O_3$ and $Tm_2O_3$ were determined from the onsets of endothermic peaks on heating and are listed in Table 1.

**Table 1.** Temperatures (° C) for C-H phase transformation and melting of $Er_2O_3$ and $Tm_2O_3$ from differential thermal analysis experiments.

| Sample | $Er_2O_3$ | | $Tm_2O_3$ | |
|---|---|---|---|---|
| Transition | C-H | H-Liq. | C-H | H-Liq. |
| First heating | 2302 | 2414 | 2391 | 2426 |
| Second heating | 2300 | 2423 | 2377 | 2406 |
| $\bar{x} \pm 2\delta\bar{x}$ | 2301 ± 2 | 2419 ± 9 | 2384 ± 14 | 2416 ± 20 |

The temperature for the C-H transition in $Er_2O_3$ was reproduced to be 2301 ± 2 °C on two heating measurements with different sensors using 10 and 20 °/min heating rates. The uncertainty to the reported value was assigned as ± 12 °C based on reference value for melting temperature of $Y_2O_3$ used for calibration. The enthalpies of phase transformation and fusion were determined as the average from corresponding heat effects on heating and on cooling and are listed in Table 2.

**Table 2**. Enthalpies (kJ/mol) for C-H phase transformation and fusion of $Er_2O_3$ and $Tm_2O_3$ from differential thermal analysis experiments.

| Sample | $Er_2O_3$ | | $Tm_2O_3$ | |
|---|---|---|---|---|
| Transition | C-H | H-Liq. | C-H | H- Liq. |
| First heating | 39.6 | 47.7 | 78.9 | 74.5 |
| First cooling | 45.3 | 69.5 | 70.4 | 76.2 |
| Second heating | 51.0 | 58.8 | 65.9 | 60.0 |
| Second cooling | 55.5 | 60.1 | 62.7 | 63.5 |
| $\bar{x} \pm 2\delta\bar{x}$ | 48 ± 7 | 59 ± 9 | 69 ± 7 | 69 ± 8 |

Figure 3 shows the heat flow and sample temperature traces for phase transitions in $Er_2O_3$, $Tm_2O_3$ and $Y_2O_3$ on heating at the same rate (10 °C/min). The undercooling on H-C transformation in $Tm_2O_3$ experiments reached 103 degrees, and was similar to that observed for the H-C transition in $Y_2O_3$. For $Er_2O_3$ H-C transition undercooling did not exceed 57 degrees, even at 20 °C/min cooling rate (see Tables S1 and S2 in supporting information).

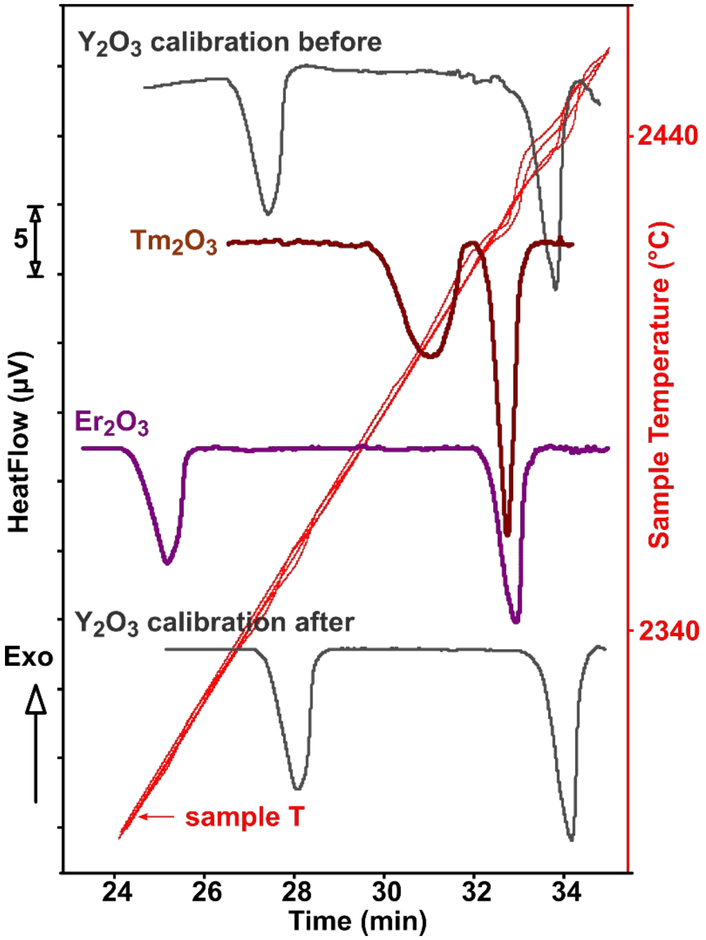

**Figure 3.** Heat flow and sample temperature traces showing C-H phase transformation and melting of $Tm_2O_3$ and $Er_2O_3$ samples in DTA in sealed W crucibles. $Y_2O_3$ standard was melted before and after the experiments (top and bottom traces, respectively) for temperature and sensitivity calibration. Baseline subtracted. See Tables S1 and S2 in supporting information for details.

### 4.2 Thermal expansion from high temperature X-ray diffraction

The thermal expansion for C-phase $Er_2O_3$ and $Tm_2O_3$ from room temperature to the C-H transition onset was determined from high temperature diffraction on levitated samples. The thermal gradient in solid laser heated aerodynamically levitated samples can reach 500 °C/mm.[43]

It varies with temperature and from sample to sample due to changes in thermal conductivity, gas flow required for levitation and sample rotation and changes in laser beam collimation at different power levels. For this reason, only mean thermal expansion from room temperature to the C-H transition temperatures was determined. The lattice parameters (*a*) of laser melted $Er_2O_3$ and $Tm_2O_3$ at room temperature were measured on the powdered samples with a silicon internal standard. The lattice parameters at transition temperatures were refined from synchrotron diffraction patterns of laser heated levitated samples, in which the H-phase reflections were present. Pawley refinement results and metrics for $Tm_2O_3$ at the C-H transition temperature are presented in Figure 4.

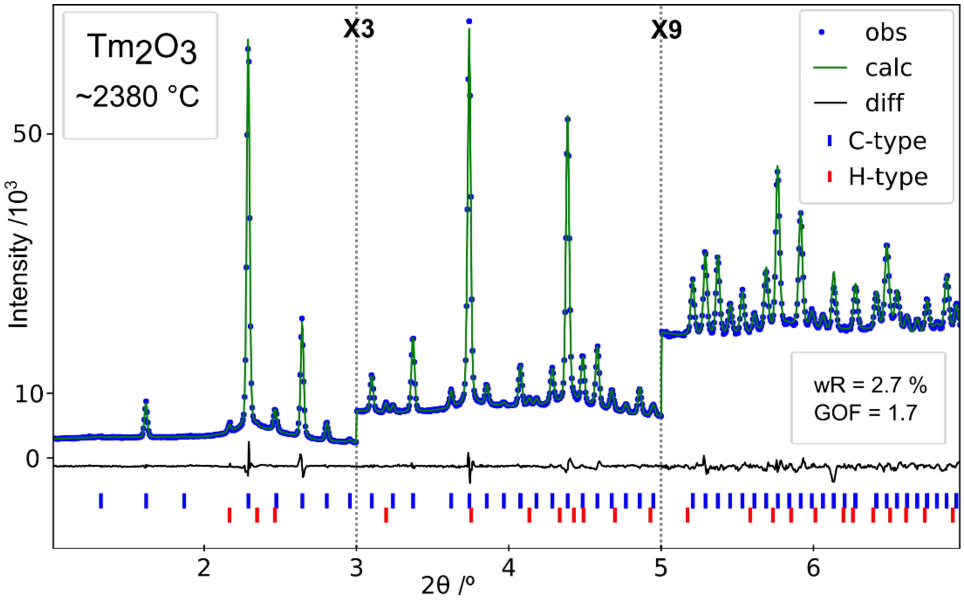

**Figure 4.** Pawley refinement of C-type $Tm_2O_3$ lattice parameter 10.7011(2) Å. The temperature of diffracted volume (2380 °C) was assigned based on appearance of H-phase peaks and C-H transition temperature measured by high temperature DTA (Table 1).

The figures with refinements for $Er_2O_3$ at C-H transition temperature and room temperature patterns are included in the supporting information (Fig. S1 and S2). The values of transitions temperatures ($T_{tr}$) determined from DTA measurements were used for calculations of mean linear thermal expansion coefficients TEC (25 °C - $T_{tr}$) = ($a_{(Ttr)} - a_{(25\ °C)}$)/($T_{tr}$ - 25 °C)/$a_{(25\ °C)}$ and are listed in Table 3 with propagated uncertainties from transition temperatures and cell parameters measurements.

**Table 3.** Lattice cell parameters of C-phase (bixbyite) of $Er_2O_3$ and $Tm_2O_3$ at room and at C-H transition temperature and mean linear thermal expansion coefficient.

| T, °C | $Er_2O_3$ $a$, Å | †wR, % | T, °C | $Tm_2O_3$ $a$, Å | †wR, % |
|---|---|---|---|---|---|
| 25 | 10.5497(1) | 6.5 | 25 | 10.4852(1) | 4.7 |
| 2300 | 10.7609(3) | 4.3 | 2380 | 10.7011(2) | 2.7 |
| TEC α, $10^{-6}$/K | 8.8 ± 0.2 | | | 8.7 ± 0.1 | |

†weighted residual from Pawley refinement

### 4.3 Ab initio molecular dynamic computations

The computational results for volume and energy for $Er_2O_3$ and $Tm_2O_3$ in the C-type structure and in the liquid state are presented in Table 4. For solid oxides, computations were performed for 25 °C and from 1827 to 2427 °C with a step of 200 °C. For liquid oxides, computations were performed from 2427 °C to 3027 °C with the same temperature step. The density and lattice cell parameters were calculated from computed volumes. The latent enthalpy of the metastable C-L transition is calculated to be 111.3 kJ/mol for $Er_2O_3$ and 114.3 kJ/mol for $Tm_2O_3$ from the energies of solid and liquid oxides computed at 2427 °C. Ab initio MD computations of the hypothetical melting temperature for C-type $Er_2O_3$ and $Tm_2O_3$ yield the values 2222 ± 55 °C and 2332 ± 85°C, respectively (Fig. S4 in supporting information).

**Table 4**. Results of ab initio MD computations (PBE) for $Er_2O_3$ and $Tm_2O_3$ on 240 atoms.

| | T °C | CPU, hours | MD length, ps | Volume, Å$^3$/atom | Energy, eV/atom | *a,* Å | Density, g/cm$^3$ |
|---|---|---|---|---|---|---|---|
| C-type $Er_2O_3$ | 25 | 19789 | 8.1 | 14.34(1) | -8.351(1) | 10.470† | 8.86(1) |
| | 1827 | 19289 | 27.5 | 15.13(1) | -7.869(3) | 10.657 | 8.40(1) |
| | 2027 | 19608 | 26.8 | 15.23(1) | -7.810(3) | 10.682 | 8.34(1) |
| | 2227 | 30415 | 31.2 | 15.37(1) | -7.748(3) | 10.712 | 8.27(1) |
| | 2427 | 18764 | 29.4 | 15.46(1) | -7.683(4) | 10.733 | 8.22(1) |
| Liquid $Er_2O_3$ | 2427 | 19812 | 32.0 | 15.50(3) | -7.452(4) | | 8.20(2) |
| | 2627 | 59381 | 65.5 | 15.70(4) | -7.379(3) | | 8.09(2) |
| | 2827 | 43351 | 53.9 | 15.94(3) | -7.301(4) | | 7.97(2) |
| | 3027 | 18279 | 29.1 | 16.11(3) | -7.231(5) | | 7.88(2) |
| C-type $Tm_2O_3$ | 25 | 19728 | 41.4 | 14.14(1) | -8.373(1) | 10.418 | 9.07(1) |
| | 1827 | 15151 | 51.3 | 14.89(1) | -7.888(3) | 10.602 | 8.60(1) |
| | 2027 | 12839 | 38.9 | 14.99(1) | -7.830(4) | 10.625 | 8.55(1) |
| | 2227 | 13627 | 47.0 | 15.10(1) | -7.768(4) | 10.651 | 8.49(1) |
| | 2427 | 17818 | 39.7 | 15.21(1) | -7.704(3) | 10.676 | 8.43(1) |
| Liquid $Tm_2O_3$ | 2427 | 21366 | 46.1 | 15.28(4) | -7.467(4) | | 8.38(2) |
| | 2627 | 54687 | 85.1 | 15.48(3) | -7.392(3) | | 8.28(2) |
| | 2827 | 46080 | 67.2 | 15.75(4) | -7.319(4) | | 8.14(2) |
| | 3027 | 30573 | 95.9 | 15.94(4) | -7.245(4) | | 8.04(3) |

†The propagated computational uncertainties in lattice parameters are ± 0.0003 Å or less, the uncertainties for the computed volume, density and energy are given in the bracket after the last significant digit.

## 5. DISCUSSION

### 5.1 Phase transition and melting temperatures

Our results indicate that both $Er_2O_3$ and $Tm_2O_3$ melt at ~2420 °C, but the temperature of pre-melting phase transformation is ~90 °C lower for $Er_2O_3$ than for $Tm_2O_3$ for which the H-phase is stable only for ~30 °C before melting. The measured C-H transition temperatures for both oxides are within uncertainties for the values chosen in Zinkevich[12] assessment, but the value for the $Tm_2O_3$ C-H transition in Konings[44] et al. assessment (2315 ± 30 °C) is significantly lower than our value from DTA experiments (2384 ± 14 °C). Konings[44] gave the recommended value for C-H transition based on Foex and Traverse[11] work. They reported cooling traces of large volumes (10

- 25 $cm^3$) of $RE_2O_3$ partially melted with a solar furnace in air, argon and hydrogen. All $RE_2O_3$ except $Eu_2O_3$ retained their composition after melting in Ar, air and $H_2$. In our cooling traces for $Tm_2O_3$ we observed thermal arrests at ~2280 °C in Ar and at ~2310 °C in $O_2$ (Fig. S4 in Supporting Information), consistent with Foex and Traverse.[11] DTA results also indicate that the H phase can be undercooled as much as 100 °C below the transition temperature measured on heating. Thus, the higher value for C-H transition in $Tm_2O_3$ (2384 ± 14 °C) measured on heating in this work is consistent with previous experiments and preferable for thermodynamic assessments.

The IUPAC report[17] on melting temperature of $RE_2O_3$ was in preparation for four years (1983-87) by an international commission on high temperature and solid state chemistry. For $Er_2O_3$ this report analyzes six experimental measurements of melting temperature from different laboratories ranging from 2364 to 2416 °C and recommends the value 2418 ± 15 °C. This is in excellent agreement with our value for $Er_2O_3$ melting temperature from DTA (2419 ± 12 °C). $Tm_2O_3$ was the only lanthanide for which no experimental measurements were included in the IUPAC report and estimated melting temperature was given as 2425 ± 20 °C, between those of $Er_2O_3$ and $Yb_2O_3$, the neighboring lanthanide sesquioxides. This value was accepted in Zinkevich[12] 2007 assessment. Melting temperature for $Tm_2O_3$ reported by Shevtchenko[45] as 2409 ± 30 °C was cited in Konings[44] 2014 assessment as the recommended value. Our experimental result for melting temperature of $Tm_2O_3$ (2416 ± 20 °C) is within uncertainties of both these values. However, it is interesting to note that $Tm_2O_3$ experimental results seem to refute the estimation of the melting temperature made from the known trend of increasing melting temperatures with atomic weight in $RE_2O_3$, and indicate that $Tm_2O_3$ melts at lower temperature than $Er_3O_3$. The value for melting temperature of $Tm_2O_3$ in the set used for training the GNN model was 10 °C lower than for $Er_2O_3$. In values estimated by the model, the difference remained and increased to 40 °C, indicating that lower melting temperature of $Tm_2O_3$ is supported from other compounds in the training dataset. The virtual melting temperatures for C-phase calculated by ab initio MD computations are close to experimental values for C-H transition temperatures and corroborate DTA results, indicating that the C-phase is stable in $Tm_2O_3$ up to the higher temperatures.

### 5.2. High temperature heat capacities from computations

The summary of data obtained from experiment and computations performed in this work is presented in Table 5. The computed lattice parameters for C-type $Er_2O_3$ and $Tm_2O_3$ are 0.8 % lower than experimental values at room temperature but only 0.5 % lower at the C-H transition temperature (Tables 4 and 5). This results in a larger mean thermal expansion from computations. The computations provide realistic 145 J/mol/K value for average heat capacity of C-type $Er_2O_3$ and $Tm_2O_3$ above 1800 °C up to the transition temperature, for which no experimental data are available.

**Table 5.** Thermal expansion, heat capacity and transition enthalpies for $Er_2O_3$ and $Tm_2O_3$ from experiment and computations.

| Phase/Property | $Er_2O_3$ | $Tm_2O_3$ | Method |
|---|---|---|---|
| C-type TEC ($\alpha$, $K^{-1}$)$\cdot 10^{-6}$ | 8.8 ± 0.2<br>10.5 ± 0.3 | 8.7 ± 0.1<br>10.3 ± 0.3 | XRD 25 °C - $T_{tr}$ (C-H)<br>AI MD at 25 °C - $T_{tr}$ (C-H) |
| C-type $C_p$ J/mol/K | 146 ± 5 | 144 ± 6 | AI MD 1827-2027 °C |
| $T_{tr}$ (C-H), °C | 2301 ± 12 | 2384 ± 14 | Differential Thermal Analysis (DTA) experiments* |
| $\Delta H_{trs}$ (C-H), kJ/mol | 48 ± 7 | 69 ± 7 | |
| $T_{fus}$ (H-L), °C | 2419 ± 12 | 2416 ± 20 | |
| $\Delta H_{fus}$(H-L), kJ/mol | 59 ± 9 | 69 ± 8 | |
| $\Delta H_{C\text{-}L}$, kJ/mol | 111 ± 1 | 114 ±2 | AI MD at 2427 °C |
| Liq. density, g/cm$^3$ | 8.17 ± 0.16[46]<br>8.20 ± 0.02 | 8.3 ± 0.1[47]<br>8.38 ± 0.02 | Experiment (ESL at ISS)[46, 47]<br>AI MD at 2427 °C |
| Liq. $C_p$, J/mol/K | 178 ± 5 | 178 ± 4 | AI MD at 2427 – 3027 °C |

* See Table S3 in supporting information for the comparison with previous reports.

The sum of the enthalpies of measured C-H transitions and fusion can be correlated with energy of C-L transition from ab initio MD. For $Er_2O_3$ the values agree within experimental uncertainty, for $Tm_2O_3$ the sum of experimental enthalpies is 24 kJ/mol larger. Due to limited number of experiments performed, it is not clear if experimental or computed value is more reliable in this case. The computed density of liquid $Er_2O_3$ and $Tm_2O_3$ at 2427 °C (~10 °C above experimental melting temperatures) are 8.20 and 8.38 g/cm$^3$, respectively. They are in remarkable agreement with the measurements recently performed at the International Space Station by in situ videography of laser heated levitated molten oxides[46, 47] (8.2 ± 0.2 for $Er_2O_3$[46] and 8.3 ± 0.1 and $Tm_2O_3$[47]). This renders confidence in the computational results for the average value heat capacity of liquid $Er_2O_3$ and $Tm_2O_3$ 178 ± 5 J/mol/K for the range 2427 – 3027 °C.

### 5.3. Enthalpies and entropies of C-H transition and fusion

Enthalpies of pre-melting cubic-hexagonal phase transformations and fusions of $Er_2O_3$ and $Tm_2O_3$ are listed in Table 5. These are the first experimental measurements for these oxides. The transition and melting temperatures were measured by DTA on heating. Metastability, while common on cooling, is rarely observed on heating. By assigning $\Delta G = 0$ at the transition and melting temperatures, entropies of C-H transition and fusion can be calculated as $\Delta H/T$ (K). This results in values for $\Delta S_{\text{C-H}}$ 18.6 ± 0.1 and 26.0 ± 0.1 and $\Delta S_{fus}$ 21.9 ± 0.2 and 25.6 ± 0.1 J/mol/K for $Er_2O_3$ and $Tm_2O_3$, respectively (Table S3). The small values for fusion entropies suggest that H-phase stable before melting is highly disordered. They are comparable to the fusion entropies of cubic $ZrO_2$, YSZ and $HfO_2$ (18 to 20 J/mol/K),[48, 49] in which oxygen atomic displacement parameters and diffusion coefficients comparable with liquid phase data were reported from in situ neutron diffraction studies[50] and ab initio computations.[49]

Zinkevich[12] and Konings et al.[44] assessments of C-H and fusion enthalpies for $Er_2O_3$ and $Tm_2O_3$ are based on entropy changes assigned to transitions in $Y_2O_3$ from drop calorimetry experiments by Shpil'rain et al.[14] This resulted in smaller estimated enthalpies and entropies for C-H transition and larger for fusion (Table S3 in supporting information). However, in drop calorimetry experiments on $Y_2O_3$ C-H transition and melting were not well resolved[14] and separation of heat effect between them is somewhat arbitrary. The recent measurements and ab initio computations[20] of fusion enthalpy of $Y_2O_3$ are within experimental uncertainties of Shpil'rain[14] results, however, the ratio of heat effects related to fusion and C-H transformation from DTA measurements[42, 51] indicated larger C-H transition enthalpy and entropy[20] and are in good agreement with new results for $Er_2O_3$ and $Tm_2O_3$.

### 5.4. Thermal expansion

The experimental data on thermal expansion of binary oxides available by 1984 were reviewed by Taylor.[52] The comprehensive investigation of $RE_2O_3$ by high temperature X-ray diffraction at 25 - 1300 °C was performed in the U.S. Bureau of Mines by Stecura and Campbell.[53] The high temperature unit cell parameters for $Er_2O_3$ were also reported by Singh and Dayal[54] and by Saiki et al.[55] The unit cell parameters for Er and Tm sesquioxides measured in this work at room temperature and at C-H transition temperatures are plotted in Figure 5 in comparison with previous studies which were limited to ~1300 °C. The mean linear thermal expansion coefficients (TEC, $\alpha$) for 25 -1300 °C range calculated from published data are $8.4 \pm 0.1$ and $8.6 \pm 0.1$ ($\cdot 10^{-6}$/K) for $Er_2O_3$ and $Tm_2O_3$, respectively. They are only slightly lower than $\alpha$ values obtained in this work for $Er_2O_3$ in 25 – 2300 °C range and for $Tm_2O_3$ in 25 – 2380 °C range ($8.8 \pm 0.2$ and $8.7 \pm 0.1$ ($\cdot 10^{-6}$/K)). The computational results provide higher absolute values for TEC but also do not indicate sharp increase in thermal expansion at high temperature. This is in a drastic contrast with behavior of fluorite,[56] and defect fluorite phases in proximity of melting temperature (e.g. 3-fold increase in TEC was reported[50] for YSZ in the last 200 °C of the stability range). Thermal expansion coefficients for $Er_2O_3$ and $Tm_2O_3$ are slightly higher than those reported for C-type $Lu_2O_3$ and $Yb_2O_3$ (7.7 ± 0.6 and 8.5 ± 0.6 ($\cdot 10^{-6}$/K), respectively for the range from 25 °C to melting temperatures) and slightly lower than for $Y_2O_3$ (9.0 ± 0.2 ($\cdot 10^{-6}$/K) from 25 °C to C-H transition temperature)[57]. The differences are close to uncertainties, however, the expected general correlation of lower thermal expansion coefficients with larger temperature stability range of C-phase is observed. The relative linear thermal expansion of C-phase in Lu, Yb, Tm, Er and Y sesquioxides from 25 °C to melting or C-H transition temperature is 2.0 ± 0.1% (2.00 % for $Er_2O_3$, 2.06 % for $Tm_2O_3$, 1.93 % for $Lu_2O_3$, and 2.1 % for $Yb_2O_3$ and $Y_2O_3$). This is slightly lower than the values extrapolated from the data available below 1500 °C in Taylor's 1984 review (2.25 - 2.11 %).[52]

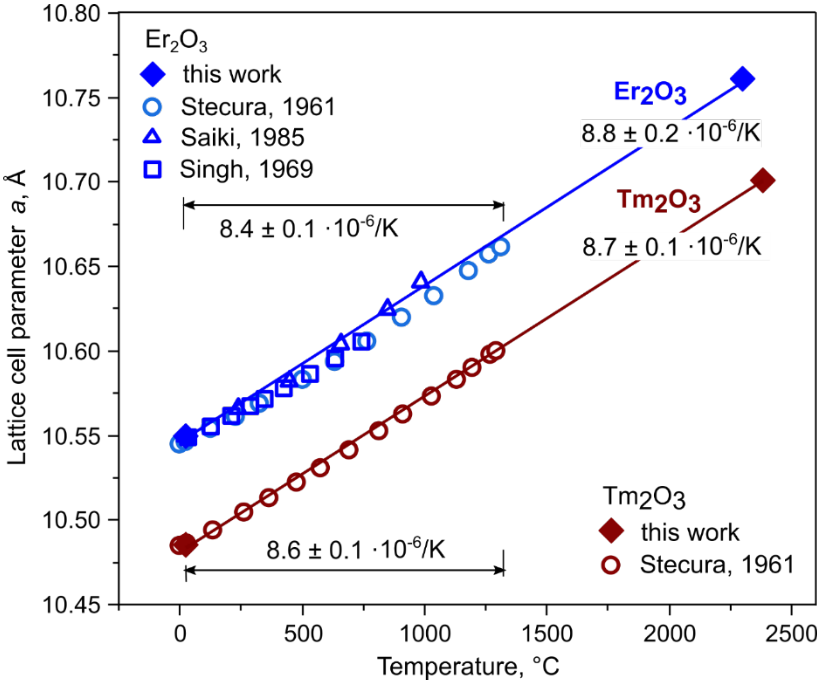

**Figure 5**. Lattice cell parameters of C-phase (bixbyite) of $Er_2O_3$ and $Tm_2O_3$ at room and at C-H transition temperatures and mean linear thermal expansion coefficients from this work compared with previously reported[53-55] data.

## 5.5. H-phase in $RE_2O_3$

H-type high temperature modification of $RE_2O_3$ was first proposed by Foex and Traverse[11] in 1966. From cooling curves and high temperature XRD they suggested that this is a high temperature phase common to all $RE_2O_3$, except $Lu_2O_3$ and $Sc_2O_3$, and noted that diffraction pattern is very similar to A-type structure in which $RE_2O_3$ from La to Nd occur at room temperature. A-type structure of $RE_2O_3$ (often referred to as hexagonal in the literature) has been debated in several X-ray[58, 59] and neutron[60, 61] diffraction studies and now it is established in a trigonal space group $P\overline{3}m1$. The existence of H-type structure for $La_2O_3$ and $Nd_2O_3$ was confirmed from high temperature neutron diffraction data by Aldebert et al.[62, 63] in space group $P6_3/mmc$. They proposed that oxygen atoms in the structure are in dynamic disorder and reported superplasticity from the observation of the solid sample creeping under its own weight in the container. The high temperature structures for other $RE_2O_3$ were not refined, thus the question whether the H-type phases of the rest of $RE_2O_3$ possess the same structure is still open.

Our DTA results show that enthalpies of C-H transition are comparable to fusion enthalpy of $Tm_2O_3$ and $Er_2O_3$ and corroborate the notion of effective melting of oxygen sublattice in H phase which indeed can induce superplasticity. The volume change on C-H transition in $Y_2O_3$ was refined as -3 % from synchrotron diffraction.[57] Our experimental and computational results indicate negative volume change of similar magnitude on C-H transition in $Er_2O_3$ and $Tm_2O_3$. They will be reported in a separate publication.

## 6. CONCLUSIONS

Thermodynamics of high temperature phase transformations and fusion of $Er_2O_3$ and $Tm_2O_3$ were studied by differential thermal analysis, thus providing new recommended values for enthalpy and entropy of phase transitions and fusion. The temperature and sensitivity calibration in 2300 – 2450 °C range was accomplished by melting $Y_2O_3$ for which enthalpy of fusion and pre-melting phase transformation were measured earlier by drop calorimetry. The thermal expansion of cubic phases was derived from synchrotron diffraction on laser heated aerodynamically levitated samples. The experimental data were used to benchmark ab initio molecular dynamic computations for cubic and liquid phases, which provided lattice cell parameters and energy as function of temperature and metastable melting temperatures for cubic phases. The computations provided high temperature heat capacities for the cubic and liquid $Er_2O_3$ and $Tm_2O_3$, which is challenging to measure directly. C-type (bixbyite) structure of rare earth sesquioxides is often described as a defect fluorite structure with ordered vacancies. However, their high temperature behavior is very different: Our results for C-type $Er_2O_3$ and $Tm_2O_3$ show no indication of the drastic increase in thermal expansion or in heat capacity before C-H transformation seen in fluorite and defect fluorite structures before melting.

## Supporting Information

The following files are available free of charge. Additional details on DTA experiments and calibrations, on AI MD computations of melting temperatures and on integration and Pawley refinement of high temperature synchrotron diffraction data, table with comparison of thermodynamic data obtained in this work with previous experimental results and assessments.

## Corresponding Authors

Qi-Jun Hong

School for Engineering of Transport, Energy and Matter, Arizona State University, Tempe, AZ; 85287, USA; qhong7@asu.edu
Alexandra Navrotsky
Center for Materials of the Universe, School of Molecular Sciences, Arizona State University, Tempe, AZ 85287, USA; anavrots@asu.edu

## Author Contributions

The manuscript was written through contributions of all authors. All authors have given approval to the final version of the manuscript.

## Funding Sources

This research was supported by the US National Science Foundation under Collaborative Research Awards DMR-2209026 (Arizona State University), and DMR-2209027 (Brown University) with use of Research Computing at Arizona State University and the Extreme Science and Engineering Discovery Environment (XSEDE), supported by the National Science Foundation (ACI-1548562). Use of the Advanced Photon Source (APS, beamline 6-ID-D), an Office of Science User Facility operated for the DOE Office of Science by Argonne National Laboratory, was supported by the DOE under Contract No. DEACO2-06CH11357.

## Acknowledgments

This research was supported by the US National Science Foundation under Collaborative Research Awards DMR-2209026 (Arizona State University), and DMR-2209027 (Brown University) with use of Research Computing at Arizona State University and the Extreme Science and Engineering Discovery Environment (XSEDE), supported by the National Science Foundation (ACI-1548562). Use of the Advanced Photon Source (APS, beamline 6-ID-D), an Office of

Science User Facility operated for the DOE Office of Science by Argonne National Laboratory, was supported by the DOE under Contract No. DEACO2-06CH11357. The high temperature diffraction experiments would not be possible without Chris Benmore and Richard Weber ensuring operation and upgrades of aerodynamic levitator at beamline 6-ID-D at APS.

## References

1. Witte, R.; Sarkar, A.; Kruk, R.; Eggert, B.; Brand, R. A.; Wende, H.; Hahn, H., High-entropy oxides: An emerging prospect for magnetic rare-earth transition metal perovskites. *Physical Review Materials* **2019,** *3* (3), 034406.

2. Smialek, J. L.; Miller, R. A., Revisiting the Birth of 7YSZ Thermal Barrier Coatings: Stephan Stecura †. *Coatings* **2018,** *8* (7), 255.

3. Adachi, G.; Imanaka, N.; Kang, Z. C., *Binary Rare Earth Oxides*. Springer Netherlands: 2006.

4. Imanaka, N.; Masui, T., Advances in direct NOx decomposition catalysts. *Applied Catalysis A: General* **2012,** *431-432*, 1-8.

5. Bünzli, J.-C. G.; Piguet, C., Taking advantage of luminescent lanthanide ions. *Chemical Society Reviews* **2005,** *34* (12), 1048-1077.

6. Goldschmidt, V. M.; Ulrich, F.; Barth, T., Geochemical distribution laws of the elements. IV. The crystal structure of the oxides of the rare earth metals. *Skrifter utgit av det norske Videnskap-Akademi i Oslo. (I) Matem.-Naturvid.* **1925,** (No. 5), pp. 5-24.

7. Rustad, J. R., Density functional calculations of the enthalpies of formation of rare-earth orthophosphates. *American Mineralogist* **2012,** *97* (5-6), 791-799.

8. Ushakov, S. V.; Hayun, S.; Gong, W.; Navrotsky, A., Thermal analysis of high-entropy rare earth oxides. *Materials* **2020,** *13* (14), 3141.

9. Pianassola, M.; Anderson, K.; Agca, C.; Benmore, C. J.; McMurray, J. W.; Neuefeind, J. C.; Melcher, C.; Zhuravleva, M., In situ high-temperature structural analysis of high-entropy rare-earth sesquioxides. *Chemistry of Materials* **2023,** *35* (3), 1116-1124.

10. Tracy, C. L.; Lang, M.; Zhang, F.; Trautmatm, C.; Ewing, R. C., Phase transformations in $Ln_2O_3$ materials irradiated with swift heavy ions. *Phys. Rev. B: Condens. Matter Mater. Phys.* **2015,** *92* (17), 174101/1-174101/14.

11. Foex, M.; Traverse, J. P., Investigations about crystalline transformation in rare earths sesquioxides at high temperatures. *Rev. Int. Hautes Temp. Refract.* **1966,** *3* (4), 429-53.

12. Zinkevich, M., Thermodynamics of rare earth sesquioxides. *Progress in Materials Science* **2007,** *52* (4), 597-647.

13. Shpil'rain, E. E.; Kagan, D. N.; Barkhatov, L. S.; Koroleva, V. V., Measurement of the enthalpy of solid and liquid phases of yttria. *High Temp. - High Pressures* **1976,** *8*, 183-6.

14. Shpil'rain, E. E.; Kagan, D. N.; Barkhatov, L. S.; Koroleva, V. V.; Coutures, J. P.; Foex, M., Investigation of fusion and phase transition enthalpies of yttrium oxide and scandium oxide. *Rev. Int. Hautes Temp. Refract.* **1979,** *15*, 249-52.

15. Ushakov, S. V.; Navrotsky, A., Direct measurements of fusion and phase transition enthalpies in lanthanum oxide. *J. Mater. Res.* **2011,** *26*, 845-847.

16. Hlavac, J., Melting temperatures of refractory oxides. Part I. *Pure Appl. Chem.* **1982,** *54*, 681-8.

17. Coutures, J. P.; Rand, M. H., Melting temperatures of refractory oxides: Part II. Lanthanoid sesquioxides. *Pure Appl. Chem.* **1989,** *61*, 1461-82.

18. Pavlik, A.; Ushakov, S. V.; Navrotsky, A.; Benmore, C. J.; Weber, R. J. K., Structure and thermal expansion of $Lu_2O_3$ and $Yb_2O_3$ up to the melting points. *Journal of Nuclear Materials* **2017,** *495* (Supplement C), 385-391.

19. Fyhrie, M.; Hong, Q.-J.; Kapush, D.; Ushakov, S. V.; Liu, H.; van de Walle, A.; Navrotsky, A., Energetics of melting of $Yb_2O_3$ and $Lu_2O_3$ from drop and catch calorimetry and first principles computations. *The Journal of Chemical Thermodynamics* **2019,** *132*, 405-410.

20. Kapush, D.; Ushakov, S.; Navrotsky, A.; Hong, Q.-J.; Liu, H.; van de Walle, A., A combined experimental and theoretical study of enthalpy of phase transition and fusion of yttria above 2000° C using "drop-n-catch" calorimetry and first-principles calculation. *Acta Materialia* **2017,** *124*, 204-209.

21. Ushakov, S. V.; Shvarev, A.; Alexeev, T.; Kapush, D.; Navrotsky, A., Drop-and-catch (DnC) calorimetry using aerodynamic levitation and laser heating. *Journal of the American Ceramic Society* **2017,** *100* (2), 754-760.

22. Felice, R. A., The spectropyrometer - a practical multi-wavelength pyrometer. *AIP Conference Proceedings* **2003,** *684* (Pt. 2), 711-716.

23. Benmore, C. J.; Weber, J. K. R., Aerodynamic levitation, supercooled liquids and glass formation. *Advances in Physics: X* **2017,** *2* (3), 717-736.

24. Pawley, G., Unit-cell refinement from powder diffraction scans. *Journal of Applied Crystallography* **1981,** *14* (6), 357-361.

25. Toby, B. H.; Von Dreele, R. B., GSAS-II: the genesis of a modern open-source all purpose crystallography software package. *J. Appl. Crystallogr.* **2013,** *46* (2), 544-549.

26. Kohn, W.; Sham, L. J., Self-Consistent Equations Including Exchange and Correlation Effects. *Phys. Rev.* **1965,** *140*, A1133.

27. Kresse, G.; Furthmuller, J., Efficiency of ab-initio total energy calculations for metals and semiconductors using a plane-wave basis set. *Comp. Mater. Sci.* **1996,** *6*, 15.

28. Blochl, P. E., Projector augmented-wave method. *Phys. Rev. B* **1994,** *50*, 17953.

29. Perdew, J. P.; Burke, K.; Ernzerhof, M., Generalized gradient approximation made simple. *Phys. Rev. Lett.* **1996,** *77*, 3865.

30. Hong, Q.-J.; van de Walle, A., A user guide for SLUSCHI: Solid and Liquid in Ultra Small Coexistence with Hovering Interfaces. *Calphad* **2016,** *52*, 88-97.

31. Nosé, S., A molecular dynamics method for simulations in the canonical ensemble. *Molecular Physics* **1984,** *52* (2), 255-268.

32. Hoover, W. G., Canonical dynamics: Equilibrium phase-space distributions. *Physical Review A* **1985,** *31* (3), 1695-1697.

33. Hong, Q.-J.; van de Walle, A., Solid-liquid coexistence in small systems: A statistical method to calculate melting temperatures. *J. Chem. Phys.* **2013,** *139*, 094114.

34. Hong, Q.-J.; van de Walle, A., Solid-liquid coexistence in small systems: A statistical method to calculate melting temperatures. *The Journal of Chemical Physics* **2013,** *139* (9), 094114.

35. Hong, Q.-J.; Schroers, J.; Hofmann, D.; Curtarolo, S.; Asta, M.; van de Walle, A., Theoretical prediction of high melting temperature for a Mo–Ru–Ta–W HCP multiprincipal element alloy. *npj Computational Materials* **2021,** *7* (1), 1.

36. Hong, Q.-J.; Ushakov, S. V.; Navrotsky, A.; van de Walle, A., Combined computational and experimental investigation of the refractory properties of $La_2Zr_2O_7$. *Acta Mater.* **2015,** *84*, 275-282.

37. Hong, Q.-J.; van de Walle, A., Prediction of the material with highest known melting point from ab initio molecular dynamics calculations. *Physical Review B* **2015,** *92* (2), 020104.

38. Hong, Q. J. Melting Temperature Predictor. https://faculty.engineering.asu.edu/hong/melting-temperature-predictor/ (accessed April 4, 2024)

39. Hong, Q.-J.; Ushakov, S. V.; van de Walle, A.; Navrotsky, A., Melting temperature prediction using a graph neural network model: From ancient minerals to new materials. *Proceedings of the National Academy of Sciences* **2022,** *119* (36), e2209630119.

40. Hong, Q.-J., Melting temperature prediction via first principles and deep learning. *Computational Materials Science* **2022,** *214*, 111684.

41. Foex, M., Study on yttrium oxide melting point. *High Temp. - High Pressures* **1977,** *9* (3), 269-82.

42. Ushakov, S. V.; Navrotsky, A., Direct measurement of fusion enthalpy of $LaAlO_3$ and comparison of energetics of melt, glass, and amorphous thin films. *Journal of the American Ceramic Society* **2014,** *97* (5), 1589-1594.

43. Thorpe, F.; Li, T.; Weber, R.; McCormack, S. J., Environmental conical nozzle levitator equipped with dual wavelength lasers. *Journal of the American Ceramic Society* **2024,** *107* (3), 2010-2023.

44. Konings, R. J. M.; Beneš, O.; Kovács, A.; Manara, D.; Sedmidubský, D.; Gorokhov, L.; Iorish, V. S.; Yungman, V.; Shenyavskaya, E.; Osina, E., The Thermodynamic Properties of the f-Elements and their Compounds. Part 2. The Lanthanide and Actinide Oxides. *Journal of Physical and Chemical Reference Data* **2014,** *43* (1), 013101.

45. Shevchenko, A. V.; Lopato, L. M., TA method application to the highest refractory oxide systems investigation. *Thermochim. Acta* **1985,** *93*, 537-40.

46. Koyama, C.; Tahara, S.; Kohara, S.; Onodera, Y.; Småbråten, D. R.; Selbach, S. M.; Akola, J.; Ishikawa, T.; Masuno, A.; Mizuno, A.; Okada, J. T.; Watanabe, Y.; Nakata, Y.; Ohara, K.; Tamaru, H.; Oda, H.; Obayashi, I.; Hiraoka, Y.; Sakata, O., Very sharp diffraction peak in nonglass-forming liquid with the formation of distorted tetraclusters. *NPG Asia Materials* **2020,** *12* (1), 43.

47. Ishikawa, T.; Koyama, C.; Oda, H.; Shimonishi, R.; Ito, T.; Paradis, P.-F., Densities of Liquid $Tm_2O_3$, $Yb_2O_3$, and $Lu_2O_3$ Measured by an Electrostatic Levitation Furnace Onboard the International Space Station. *Metals* **2022,** *12* (7), 1126.

48. Costa, G.; Harder, B. J.; Wiesner, V. L.; Zhu, D.; Bansal, N.; Lee, K. N.; Jacobson, N. S.; Kapush, D.; Ushakov, S. V.; Navrotsky, A., Thermodynamics of reaction between gas-turbine ceramic coatings and ingested CMAS corrodents. *J. Am. Ceram. Soc.* **2019,** *102* (5), 2948-64.

49. Hong, Q.-J.; Ushakov, S. V.; Kapush, D.; Benmore, C. J.; Weber, R. J. K.; van de Walle, A.; Navrotsky, A., Combined computational and experimental investigation of high temperature thermodynamics and structure of cubic $ZrO_2$ and $HfO_2$. *Scientific Reports* **2018,** *8* (1), 14962.

50. Ushakov, S. V.; Navrotsky, A.; Weber, R. J. K.; Neuefeind, J. C., Structure and thermal expansion of YSZ and $La_2Zr_2O_7$ above 1500°C from neutron diffraction on levitated samples. *Journal of the American Ceramic Society* **2015,** *98* (10), 3381-3388.

51. Ushakov, S. V.; Maram, P. S.; Kapush, D.; Pavlik, A. J., III; Fyhrie, M.; Gallington, L. C.; Benmore, C. J.; Weber, R.; Neuefeind, J. C.; McMurray, J. W.; Navrotsky, A., Phase transformations in oxides above 2000°C: experimental technique development. *Adv. Appl. Ceram.* **2018,** *117* (sup1), s82-s89.

52. Taylor, D., Thermal expansion data: III. Sesquioxides, $M_2O_3$, with the corundum and the A-, B- and C-$M_2O_3$ structures. *British Ceramic Transactions and Journal* **1984,** *83* (4), 92-8.

53. Stecura, S. C., William J., Thermal expansion and phase inversion of rare-earth oxides. *U.S. Bureau of Mines. Report of Investigations* **1961**, 1-45.

54. Singh, H. P. D., B., Precise determination of the lattice parameters of holmium and erbium sesquioxides at elevated temperatures. *Journal of the Less-Common Metals* **1969,** *18*, 172-174.

55. Saiki, A.; Ishizawa, N.; Mizutani, N.; Kato, M., Structural Change of C-Rare Earth Sesquioxides $Yb_2O_3$ and $Er_2O_3$ as a Function of Temperature. *Yogyo Kyokai-Shi* **1985,** *93*, 649-654.

56. Dworkin, A. S.; Bredig, M. A., Diffuse transition and melting in fluorite and antifluorite type of compounds. Heat content of potassium sulfide from 298 to 1260°K. *J. Phys. Chem.* **1968,** *72* (4), 1277-81.

57. Ushakov, S. V.; Navrotsky, A., Experimental approaches to the thermodynamics of ceramics above 1500°C. *J. Am. Ceram. Soc.* **2012,** *95* (5), 1463-1482.

58. Pauling, L., The crystal structure of the A-modification of the rare earth sesquioxides. *Zeitschrift für Kristallographie-Crystalline Materials* **1929,** *69* (1-6), 415-421.

59. Mueller-Buschbaum, H.; Schnering, H. G., Strukturuntersuchungen an $La_2O_3$. *Z. Anorg. Allg. Chem.* **1965,** *340* (5-6).

60. Boucherle, J. X.; Schweizer, J., Refinement of the $Nd_2O_3$ structure and determination of the neutron scattering length of neodymium. *Acta Crystallographica Section B* **1975,** *31* (11), 2745-2746.

61. Koehler, W. C.; Wollan, E. O., Neutron-diffraction study of the structure of the A-form of the rare earth sesquioxides. *Acta Crystallographica* **1953,** *6* (8-9), 741-742.

62. Aldebert, P.; Traverse, J. P., Neutron diffraction study of the high temperature structures of lanthanum oxide and neodymium oxide. *Mater. Res. Bull.* **1979,** *14* (3), 303-23.

63. Aldebert, P.; Dianoux, A. J.; Traverse, J. P., Neutron scattering evidence for fast ionic oxygen diffusion in the high temperature phases of lanthanum oxide. *J. Phys. (Orsay, Fr.)* **1979,** *40* (10), 1005-12.

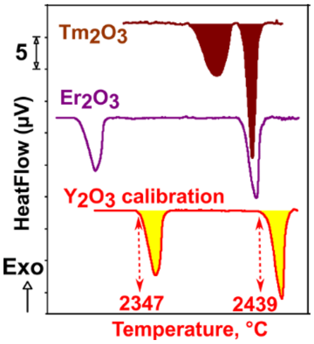

**For Table of Contents Only**